PERGAMON

International Journal of Heat and Mass Transfer 41 (1998) 4259–4279

International Journal of HEAT and MASS TRANSFER

Transient analysis of incompressible flow through a packed bed

A. Amiri, K. Vafai*

Department of Mechanical Engineering, The Ohio State University, Columbus, OH 43210, U.S.A.

Received 23 October 1997; in final form 10 March 1998

Abstract

The present investigation aims at numerically simulating the temporal energy transport for incompressible flows through a packed bed. The governing equations are formulated according to the volume averaging method. The generalized momentum equation which accounts for the inertial and viscous forces was used to carry out this research, whereas the two-energy equation model was used for simulating the energy transport. The implications of the non-Darcian terms and the thermal dispersion effects on the transient energy transport were explored. Error maps were introduced for a wide range of flow conditions and bed configurations. In addition, the investigation also tackles the applicability of the local thermal equilibrium condition and the one-dimensional approach for studying the thermal response in packed bed.

Nomenclature

a_{sf} specific surface area of the packed bed [m^{-1}]
c specific heat at constant pressure [J kg^{-1} K^{-1}]
d_p sphere particle diameter [m]
dP/dx pressure gradient [Nm^{-3}]
D_h hydraulic diameter [m]
Da Darcy number [K_∞/H^2]
F geometric function defined in equation (6)
h_{sf} solid-to-fluid heat transfer coefficient [W m^{-2} K^{-1}]
H height of the packed bed [m]
J unit vector oriented along the pore velocity vector [$\mathbf{v}_p/|\mathbf{v}_p|$]
k thermal conductivity [W m^{-1} K^{-1}]
K permeability [m^2]
L length of the packed bed [m]
Nu Nusselt number
Pr Prandtl number (ν_f/α_f)
Re_p particle Reynolds number ($u_D d_p/\nu_f$)
t time [s]
T intrinsic average temperature [K]
u velocity vector in the x-direction [m s^{-1}]
u_D Darcian velocity ($-K_\infty/\mu_f\,(dP/dx)$)
v velocity vector [m s^{-1}]
x, y cartesian coordinates [m].

Greek symbols

α thermal diffusivity [m^2 s^{-1}]
ε porosity
η dimensionless normal length scale ($y\varepsilon_\infty/K_\infty$)
μ dynamic viscosity [kg m^{-1} s^{-1}]
ν kinematic viscosity [m^2 s^{-1}]
θ dimensionless fluid phase temperature $(T_w-T_f)/(T_w-T_m)$
Ω dimensionless solid phase temperature $(T_w-T_s)/(T_w-T_m)$
ρ density [k gm^{-3}]
τ dimensionless time (u^*t/L)
ξ dimensionless axial length scale (x/L).

Subscripts

e inlet
f fluid
feff effective property for fluid
in initial
m mean
s solid
seff effective property for solid
w wall
∞ asymptotic free stream.

* Corresponding author. Tel.: 001 614 292 6560; fax: 001 614 292 3163; e-mail: vafai.1@osu.edu

0017–9310/98 $19.00
PII: S0017–9310(98)00120–3

Superscripts
f fluid
s solid
* reference quantity.

Symbol
$\langle\,\rangle$ volume-averaged quantity.

1. Introduction

Many industrial processes rely on the utilization of porous media as an effective mean for transporting and storing energy. Due to the large surface-to-volume ratio, the thermal response of these units is relatively fast as compared to other developed energy carrier devices. Common examples of industrial applications include management of geothermal systems, heat pipes, phase change applications and transpiration cooling. In addition, new technologies are thriving on utilizing porous layers and insertions to serve as a heat sink medium. Such applications are cited in Tien and Vafai [1] and Amiri and Vafai [2]. Moreover, solid insertions made of silicon or silicon carbide are reported to enhance the heat transfer in cryogenic applications. Kuzay [3] reported that the presence of these insertions may increase such systems capability to attain wall heat flux levels up to 80 MW m^{-2}.

Due to the complexity of a porous medium, the point 'microscopic' governing equations are integrated over a representative elementary volume to arrive at the 'macroscopic' level of the transport equations. The representative elementary volume, which includes both the fluid and the solid phases, needs to be much smaller than the global dimension but large enough to include the individual phases. This technique is known as the volume-averaging method and is considered in formulating the transport equations in porous media. The mechanisms associated with transferring heat between the fluid and the solid is complex and requires incorporating pertinent effects to convective flows in porous media. Vafai and Tien [4] have formulated a general mathematical model that takes into consideration the effects which causes the deviation of fluid motion from the familiar Darcy's law. These effects are referred to as the non-Darcian effects. The authors discussed the potential of the non-Darcian effects under steady state condition. Moreover, the presence of an impermeable wall next to a porous medium introduces a high porosity region adjacent to the wall [5]. As a result, the velocity reaches its maximum value near the wall and flow channeling is observed [6]. Many studies have considered the porosity maldistribution and the channeling effect and have reported on its implication on the flow dynamic and thermal behaviors in different capacities [7–12].

Another factor influencing the rate of heat transfer is the generation of small eddies in the fluid as it flows through the tortuous passages offered by the solid structure, which significantly enhances mixing of local fluid particles. The augmentation of heat transfer in part by means of mixing is known as thermal dispersion. The additional increase in convected energy is generally modeled as a diffusive flux added to the thermal diffusion term. A number of experimental investigations have proposed correlations for the modeling of thermal dispersion [13–15]. The contribution of the axial thermal dispersion to the overall thermal capacity was found to diminish at high flow rates [16–18]. Amiri and Vafai [19] have illustrated the significance of the longitudinal and the transverse thermal dispersion effects for a wide range of particle Reynolds and Darcy numbers under steady state condition.

A review of literature indicates that it is a common practice to employ the local thermal equilibrium (LTE) condition, which implies that the local temperature difference between the fluid and solid phases is negligible at all locations in the considered system. Accurate simulation of heat transfer in a porous medium requires formulating the fluid and the solid phases by separate energy equations (two-equation model) with an additional term in each equation to account for the energy exchange between them. The transient response of the solid structure is crucial to the performance of packed beds when used for thermal storage applications. The solid-to-fluid heat transfer coefficient (h_{sf}) is a major resistance to heat transfer at the interface between the fluid and the solid matrix. The coefficient h_{sf} may be determined either experimentally [20] or using semi theoretical work [21]. Schumann [22] introduced a basic analytical solution for the case of a one dimensional, semi infinite bed that is initially at a uniform temperature. The diffusion terms were ignored to arrive at predictions of the mean fluid and solid temperatures as a function of the axial position and time. The analytical solution employs Darcy's equation and has been used in analyzing thermal storage packed beds. Subsequent simplified analytical, numerical and experimental results were reviewed by Beasley and Clark [23]. However, the literature review reveals that many assumptions have been imposed restricting such solutions to a very limited number of applications. Such assumptions may include: neglecting one or more of the non-Darcian terms, dropping the thermal dispersion effects, considering a one-dimensional approach and employing the LTE condition. It is worth noting that some of these assumptions are made intuitively and without a sound physical justification [24].

In the present work, a rigorous and flexible model is initialized to explore the heat transfer aspects in a packed bed made of randomly oriented spherical particles. The investigation will shed light on the temporal impact of the non-Darcian terms and the thermal dispersion effects. In addition, the undergoing investigation will examine

the LTE condition and the one-dimensional approach under transient condition. The investigation will be carried out by formulating dimensionless variables that will serve as instruments in depicting the pertinent characteristics of energy transport in a packed bed.

2. Analysis

The problem under consideration is schematically depicted in Fig. 1. The bed is assumed long enough in the z-direction so that the problem retains two-dimensional characteristics. The solid sphere particles are of uniform shape and undeformable. The natural and radiation modes of heat transfer are assumed negligible due to the high flow rates and the moderate magnitude of the operating temperatures considered in this investigation.

2.1. *Governing equations*

The governing equations are developed using the volume-averaged method [25] and are presented based on Amiri and Vafai [19] as follows:

Continuity equation

$$\nabla\cdot\langle\mathbf{v}\rangle = 0 \tag{1}$$

Momentum equation

$$\frac{\rho_f}{\varepsilon}\left[\frac{\partial\langle\mathbf{v}\rangle}{\partial t}+\langle(\mathbf{v}\cdot\nabla)\mathbf{v}\rangle\right] = -\frac{\mu_f}{K}\langle\mathbf{v}\rangle-\frac{\rho_f F\varepsilon}{\sqrt{K}}[\langle\mathbf{v}\rangle\cdot\langle\mathbf{v}\rangle]J + \frac{\mu_f}{\varepsilon}\nabla^2\langle\mathbf{v}\rangle-\nabla\langle P\rangle^f \tag{2}$$

Fluid phase energy equation

$$\varepsilon\langle\rho_f\rangle^f c_f\frac{\partial\langle T_f\rangle^f}{\partial t}+\langle\rho_f\rangle^f c_f\langle\mathbf{v}\rangle\cdot\nabla\langle T_f\rangle^f = \nabla\cdot[k_{feff}\cdot\nabla\langle T_f\rangle^f]+h_{sf}a_{sf}[\langle T_s\rangle^s-\langle T_f\rangle^f] \tag{3}$$

Solid phase energy equation

$$(1-\varepsilon)\rho_s c_s\frac{\partial\langle T_s\rangle^s}{\partial t} = \nabla\cdot[k_{seff}\cdot\nabla\langle T_s\rangle^s]-h_{sf}a_{sf}[\langle T_s\rangle^s-\langle T_f\rangle^f] \tag{4}$$

where ε is the porosity, F is the geometric function, K is the permeability, μ_f is the fluid dynamic viscosity, $\mathbf{J}=\mathbf{v}_p/|\mathbf{v}_p|$ is the unit vector oriented along the pore velocity vector $\mathbf{v}_p$, $\langle P\rangle^f$ the average pressure read off a pressure gauge, c_f and c_s are fluid and solid specific heats at constant pressure respectively, k_f and k_s are the thermal conductivities of the fluid and solid phase respectively, ρ_f and ρ_s are the fluid and solid densities respectively, and $\langle T_f\rangle^f$ and $\langle T_s\rangle^s$ are fluid and solid intrinsic phase average temperatures respectively. Vafai and Tien [4] have indicated that the flow develops after a short entrance length and thus the convective term $\langle(\mathbf{v}\cdot\nabla)\mathbf{v}\rangle$ causing boundary layer growth can be neglected for most practical engineering cases. In eqn (2), the first term on the right-hand side resembles the frictional resistance due to the presence of the porous structure, whereas the second term on the right-hand side accounts for the inertial effects. The third term on the right-hand side represents the viscous effects introduced by the presence of an interface region. Although the momentum boundary layer is in general

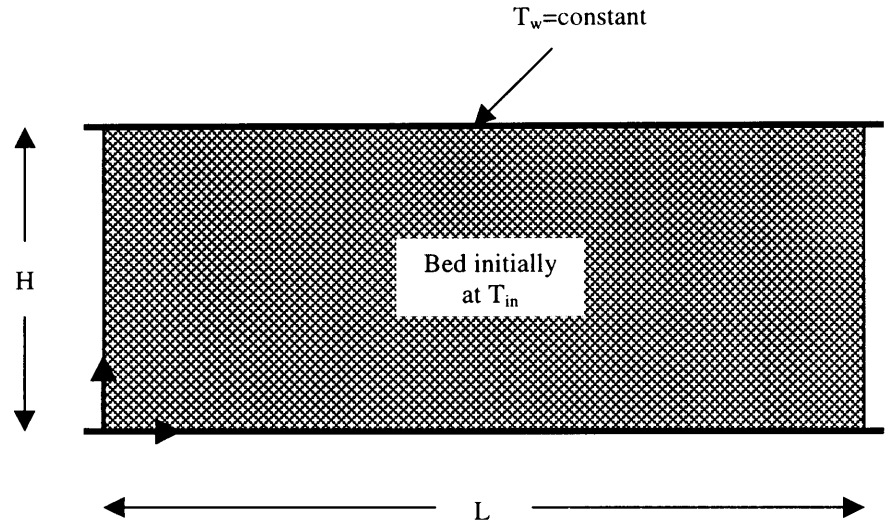

Fig. 1. Schematic diagram of the problem under consideration.

confined to a small distance from the wall, its inclusion in the analysis is crucial for computing the wall heat transfer coefficient.

The flow is driven by an imposed pressure difference in the axial direction. The permeability of the packed bed K is

$$K = \frac{\varepsilon^3 d_p^2}{150(1-\varepsilon)^2} \tag{5}$$

while the geometric function F in the momentum equation is based on the experimental findings of Ergun [26] and may be written as a function of porosity ε and particle diameter d_p as given by Vafai [27]

$$F = \frac{1.75}{\sqrt{150\varepsilon^3}}. \tag{6}$$

The porosity distribution in a packed bed is modeled by an exponential decaying function since the oscillations close to the wall are generally insignificant to heat transfer results [19]. The exponential function is generally expressed as follows

$$\varepsilon = \varepsilon_\infty[1 + a\exp(-by/d_p)]. \tag{7}$$

The free stream porosity value ε_∞ was taken as 0.37. In addition, the parameters a and b were assigned the value of 1.7 and 6.0 respectively to closely match the experimental data [5]. The specific surface area of the packed bed can be expressed as suggested by Dullien [28]

$$a_{sf} = \frac{6(1-\varepsilon)}{d_p}. \tag{8}$$

The fluid effective thermal conductivity consists of the stagnant and the dispersion conductivity and is constructed based on the experimental findings of Wakao and Kaguei [14] as follows:

$$k_{feff})_x/k_f = \varepsilon + 0.5\left(\frac{\rho_f \mathbf{u} d_p}{\mu_f}\right)Pr \tag{9}$$

$$k_{feff})_y/k_f = \varepsilon + 0.1\left(\frac{\rho_f \mathbf{u} d_p}{\mu_f}\right)Pr \tag{10}$$

where Pr is the Prandtl number. The solid effective thermal conductivity has a stagnant component only since it is stationary

$$k_{seff} = (1-\varepsilon)k_s. \tag{11}$$

Based on a number of experimental findings, Wakao et al. [20] have proposed a correlation for the solid-to-fluid heat transfer coefficient in a packed bed. The correlation covers Re_p up to 8500 and can be expressed as

$$h_{sf} = k_f\left[2 + 1.1Pr^{1/3}\left(\frac{\rho_f \mathbf{u} d_p}{\mu_f}\right)^{0.6}\right]/d_p. \tag{12}$$

The Nusselt number is defined separately for each phase based on the two-equation model and is given by

$$Nu_f = \frac{-k_{feff}[\partial\langle T_f\rangle^f/\partial y]_{y=0}}{(T_w - T_m)}\frac{D_h}{k_f} \tag{13}$$

$$Nu_s = \frac{-k_{seff}[\partial\langle T_s\rangle^s/\partial y]_{y=0}}{(T_w - T_m)}\frac{D_h}{k_f} \tag{14}$$

where D_h is the hydraulic diameter, T_w is the wall temperature and T_m is the mixed mean fluid temperature defined in a similar manner to that for classical empty channel flows.

2.2. *Boundary conditions*

In this study, no slip velocity condition is imposed at the wall. The channel walls are subjected to a constant wall temperature and the bed assumes an initial temperature that is lower than the inlet and the wall temperature. In addition, the solid temperature at the entrance was calculated directly from eqn (4) since the corresponding fluid temperature is known at the entrance. The grid points at the exit were computed via a linear extrapolation from the preceding two grid points in the flow direction. The boundary conditions are mathematically expressed as

(I) Initial condition

$$t = 0 : 0 < x \leqslant 1 \text{ and } 0 < y < 1, \mathbf{u} = 0 \text{ and } T_f = T_s = T_{in} \tag{15}$$

(II) Boundary conditions ($t > 0$)

$$x = 0 \text{ and } 0 \leqslant y \leqslant 1 : T_f = T_e \tag{16}$$

$$y = 0, H \text{ and } 0 \leqslant x \leqslant 1 : \mathbf{u} = 0 \text{ and } T_f = T_s = T_w \tag{17}$$

2.3. *Physical conditions for the numerical runs*

Solid particle diameters ranging between 2 and 8.5 mm were used to carry out the numerical runs. The thermophysical properties were evaluated at the average film temperature and were chosen merely to cover a wide range of solid-to-fluid thermal diffusivity ratios. The properties are not expected to be sensitive to the variation in temperature over the operating temperature range considered for this investigation. Table 1 lists a range of fluid and solid phase thermophysical properties that are used in this investigation. The physical values of the initial and wall temperatures were taken as

$T_{in} = 290\,\text{K}$, $T_e = 300\,\text{K}$ and $T_w = 350\,\text{K}$.

3. Solution methodology

The numerical scheme is based on finite difference method. Variable non-uniform grid size was employed in the y-direction while the grid size in the x-direction was

Table 1
Properties considered in the investigation

	(a) Fluid phase			
	ρ_f	c_f	k_f	μ_f
Air	1.08	1008	0.028	2.2×10^{-5}
Water	987	4182	0.645	52.8×10^{-5}
Engine oil	869	2014	0.142	11.2×10^{-2}
	(b) Solid phase			
	ρ_s	c_s	k_s	
TiO_2	4157	733	8	
Be	1850	1916	190	
SiC	3160	726	420	

kept constant. Refinement of the grid distribution near the wall was crucial to achieve accurate resolution for the independent variables. The compound interest grid was used such that

$$\Delta y_j = \gamma \Delta y_{j-1}. \tag{18}$$

A γ value of 1.02 was found to yield accurate results for the computational runs. As noted earlier, the study under investigation pertains to forced convection and, thus, the momentum equation is solved independently to yield the velocity field.

Explicit scheme was used to predict the transient velocity field with central difference approximation for the diffusion term. It was found from the numerical experimentation that the time interval to reach steady state was very short without much noticed difference from the steady state form of eqn (2). This fact can be used to gain significant reduction in the computational time without affecting the outcome of the energy equations to a notable extent. The tridiagonal set of algebraic equations was then solved using Gauss elimination to yield a velocity field for the first iteration. The procedure was repeated until a convergence criterion of 10^{-5} was satisfied. The vertical mesh size was varied until a velocity profile that is grid independent and smooth was obtained.

The alternating-direction implicit (ADI) method was used for the solution of the energy equations. Second-order accurate central difference was used for all spatial derivatives except for the convective term, which was approximated by an upwind difference scheme. The upwind difference was found to exhibit numerical stability even at large Peclet numbers. At grid points on the right boundary, a second order accurate three-point backward difference scheme was employed for all the spatial x-derivatives. A systematic increase in the computational length of the bed was performed until the numerical results within the physical domain were no longer affected. The independent variable in the source term in each energy equation was split between the axial and transverse diffusive terms to increase the diagonal dominance in the tridiagonal matrix at each time step.

The variation in the number of the grid points near the wall was found to have a significant impact on the fluid and solid phase temperature profiles and, as a result, on the estimation of the Nusselt number when the variable porosity and the dispersion effects were incorporated. The stability of the numerical scheme was tested by increasing the number of grid points in both directions to ensure a proper combination of Δx, Δy and Δt. A systematic decrease in the grid size was employed and a 101×141-grid configuration was found to provide grid independent results. The calculations were performed using 40 points in the near-wall region and 60 points in the main flow. Steady-state conditions were assumed when the change in the maximum norm of the converging solution between two consecutive time steps was less than 0.01. It is worth noting that the computational time runs extremely high for $Pr < 1.0$.

4. Results and discussion

The numerical algorithm was checked against some pertinent analytical and numerical solutions. The verification was achieved in two steps. First, the numerical results were checked against the analytical solution of Riaz [29]. The numerical algorithm was adjusted such that it accommodates the assumptions considered in Riaz's work including the assumption of a constant porosity medium. Air and copper were chosen as the fluid and solid phases respectively. In addition, the following parameters were used: $\varepsilon = 0.90$, $d_p = 1$ mm and $Re_p = 20$. Figure 2 shows such a comparison in terms of the dimensionless variables that appear in the work of Riaz [29]. As can be seen from the figure, the comparison displays excellent agreement between the two solutions. Second, a comparison was made between the present transient numerical findings at steady state and the numerical solution reported by Amiri and Vafai [19] for steady state analysis using a different numerical code based on the successive over relaxation method (SOR). The following values were incorporated: $Da = 3.4\times10^{-7}$, $Re_p = 100$ and $\alpha_s/\alpha_f = 32$. Comparison of fluid temperature is presented in Fig. 3 since the solid temperature shows similar trends at steady state. Again, the comparison displays excellent agreement between the two numerical methods.

In the undergoing investigation, fluid and solid centerline temperature fields and Nusselt number predictions are presented along the axial coordinate. The variables are presented in dimensionless forms as: $\xi = x/L$, $\tau = \mathbf{u}^* t/L$, $\theta = (T_w - T_f)/(T_w - T_m)$ and $\Omega = (T_w - T_s)/(T_w - T_m)$.

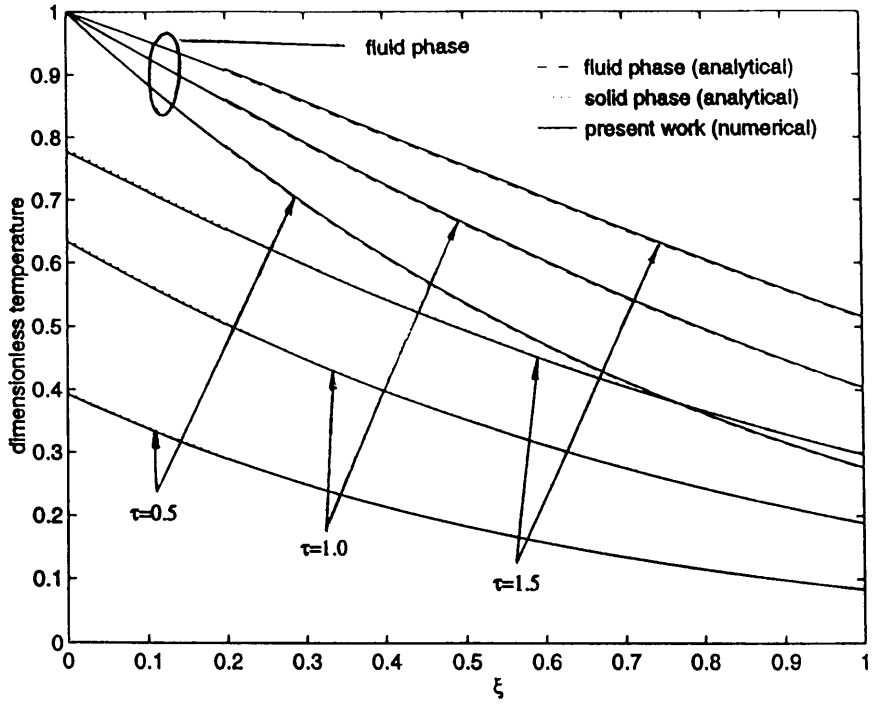

Fig. 2. Comparisons of the temperature distributions of the present work against the analytical solution of Riaz [29].

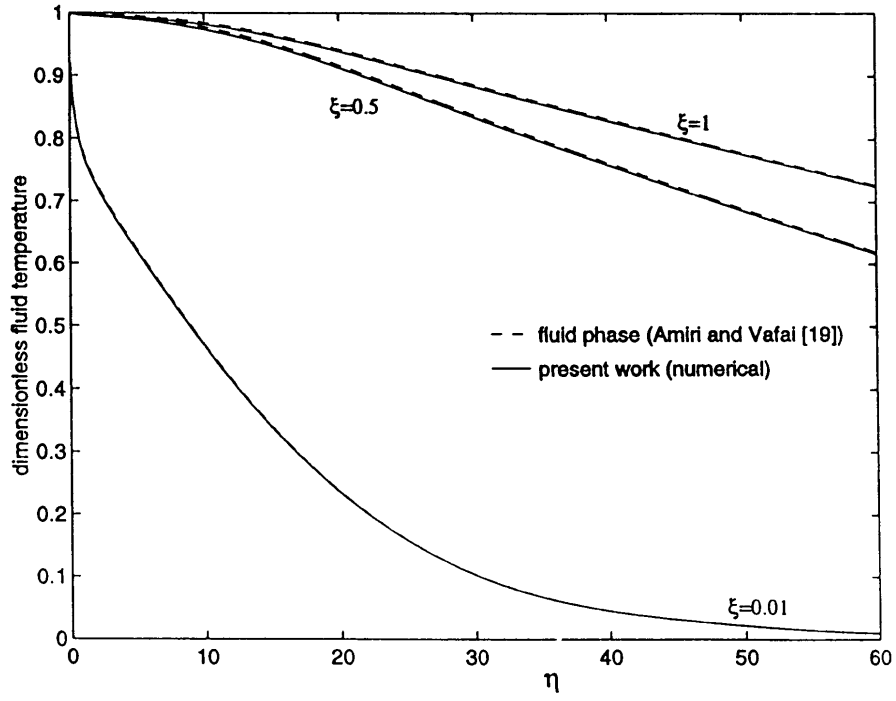

Fig. 3. Comparison of fluid temperature distribution of the present work against the numerical solution of Amiri and Vafai [19].

4.1. *Non-Darcian effects*

In exploring the temporal non-Darcian effects, the thermal dispersion effect was incorporated in the different models considered in the analysis, i.e. Darcy, modified-Darcy, generalized model without inertial effects and the generalized model. This approach was adopted since the emphasis at present is on the significance of neglecting one or more of the non-Darcian terms from the momentum equation. The implication of the non-Darcian effects on the thermal behavior of packed beds is presented in Figs 4 and 5. The following physical values were used: $\alpha_s/\alpha_f = 32$, $Da = 8.51 \times 10^{-8}$ and $Re_p = 40$. The effects of variation of these parameters are discussed later on. As can be seen from Fig. 4 the temperature for both phases increases as τ increases indicating higher heat transfer rate. The solid temperature experiences a rapid change near the entrance at early time owing to its sudden exposure of the bed to a higher temperature. This temperature elevation decays as time progresses allowing more energy to travel further down into the bed. It is worth pointing out that the oscillation in the solid temperature at early times was found to dampen when a larger solid heat capacity was incorporated. The difference in temperature between the fluid and solid phases narrows and remains almost constant as τ approaches steady state condition.

To gain more insight into the temporal non-Darcian effects over a wide range of Re_p and Da, error maps are presented. The total Nusselt number, which is simply the summation of the Nusselt number for the two phases, was chosen to compare the outcome for the different models discussed here. Taking the generalized model that accounts for all the effects as a basis, comparisons with the values obtained by using other simplified models that drops a non-Darcian effect or more were made for a given Da and Re_p. The percentage error involved in calculating the Nusselt number at a given τ was then found from

$$\% \text{ error} = \frac{|Nu_{tot}(\text{generalized model}) - Nu_{tot}(\text{simplified model})|}{Nu_{tot}(\text{generalized model}))} \times 100 \tag{19}$$

Solid-to-fluid thermal diffusivity ratios of 32 and 2256 were examined for different τ values. The comparisons are presented in Figs 6 and 7. The numbers in the parenthesis represent the estimated error in using the Darcy model, the modified-Darcy model and the generalized model that neglects the inertial effects respectively as compared to the generalized model. The figures indicate that, in general, as the Da and Re_p increase, the computed percentage error increases too. In addition, the Darcy model overpredicted the generalized model at higher Re_p values since the inertial effects in the generalized model retards the transfer of heat. The error estimated from the generalized model without the inertia effect is the highest since the magnitude of the velocity field increases substantially when channeling effect is present.

In what follows, it was found that the inertial effect retards the momentum transport, reducing the rate of heat transfer. The results imply that excluding the inertial effects would shorten the time needed to reach steady state. This is expected since the absence of the inertia effects would cause a higher flow rate, which results in more effective heat transfer between the fluid and the solid allowing steady state to be reached at a relatively shorter time. In addition, larger thermal penetration depth results from an increase in velocity magnitude caused by ignoring the inertial effects. The appreciation for the inertial effects is more pronounced at higher flow rates.

It was also found that channeling effect due to the presence of an impermeable boundary causes higher velocity, thus the set of observations made for the absence of inertial effects would be applicable to the case when the impermeable boundary is present. However, it should be pointed out that the significance of the channeling effect in enhancing energy transport is challenged by the magnitude of the inertia term. The results show that the dynamic response computed through the Darcy model may overpredict the one by the generalized model at large Re_p values. Consequently, this would make the Nusselt number estimation using Darcy's model higher compared to that estimated via the generalized model. It is important to reiterate the fact that the above statement is valid when thermal dispersion term is included in the energy equations for all the different models under consideration. One final note is that the solid phase Nusselt number is adversely affected to the change in the fluid phase Nusselt number. This is expected since the fluid and the solid phases coexist in any representative elementary volume, and based on conservation of energy; the increase in the fluid phase Nusselt number comes at the expense of a decrease in the solid phase Nusselt number.

4.2. *Transient thermal dispersion effects*

The thermal response of the packed bed during a given operating condition of the packed bed is shown in Figs 8 and 9. The results are for $\alpha_s/\alpha_f = 343$, $Da = 5.32 \times 10^{-7}$ and $Re_p = 190$. The fluid and solid temperature fields forge to the fluid mean temperature after a short distance from the entrance. The solid temperature is plotted against the logarithmic axial coordinate since it was hard to depict the initial upsurge in the solid temperature otherwise. Since dispersion conductivity is a function of the pore velocity, its magnitude reaches the maximum value very close to the wall. As may be seen in Fig. 8, the fluid temperature profile experiences a sharp gradient near the wall since diffusion becomes the dominant mode of heat transfer. This temperature gradient smooths as it

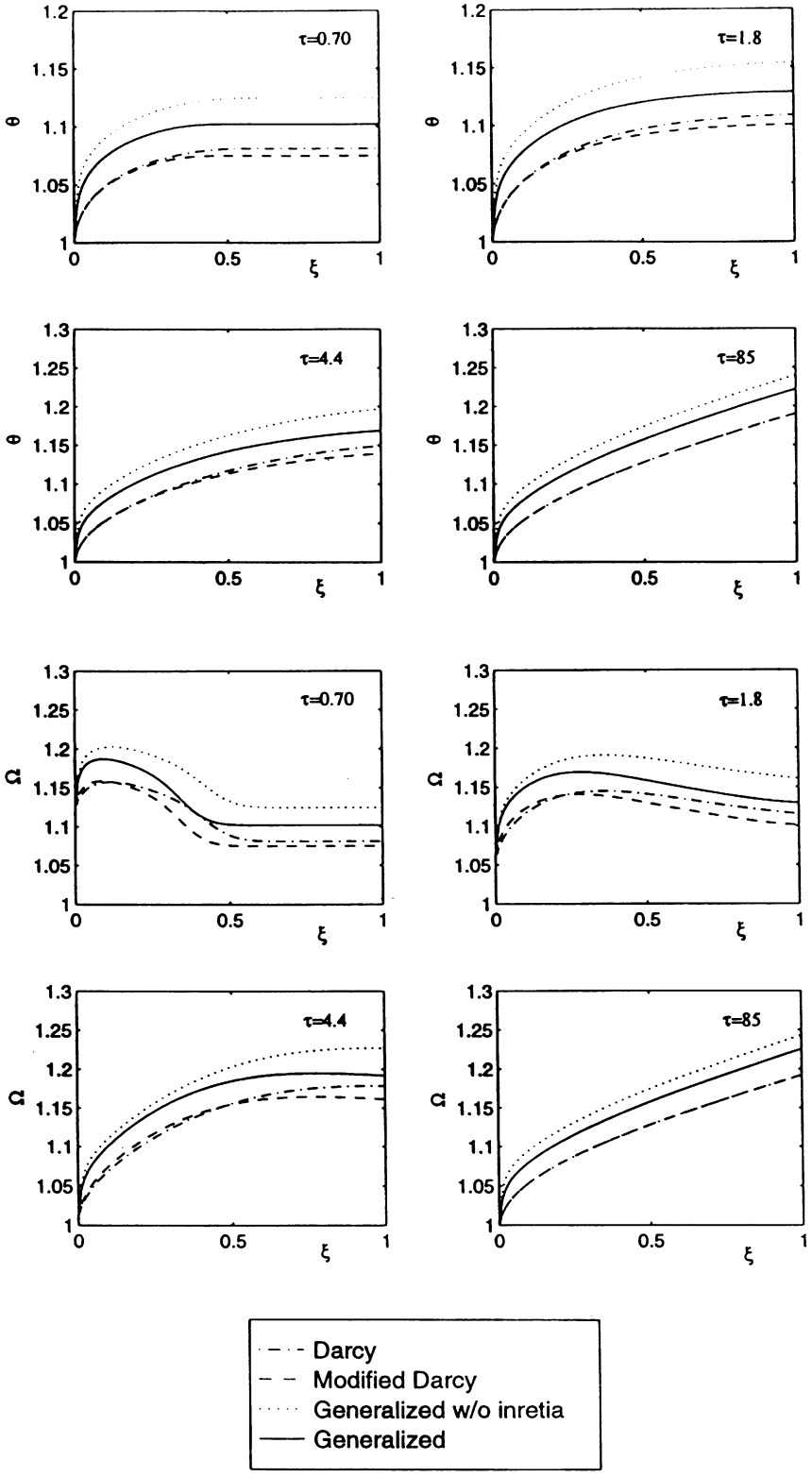

Fig. 4. Non-Darcian effects on the temporal fluid and solid phase temperature distribution for $\alpha_s/\alpha_f = 32$, $Da = 8.51 \times 10^{-8}$ and $Re_p = 40$.

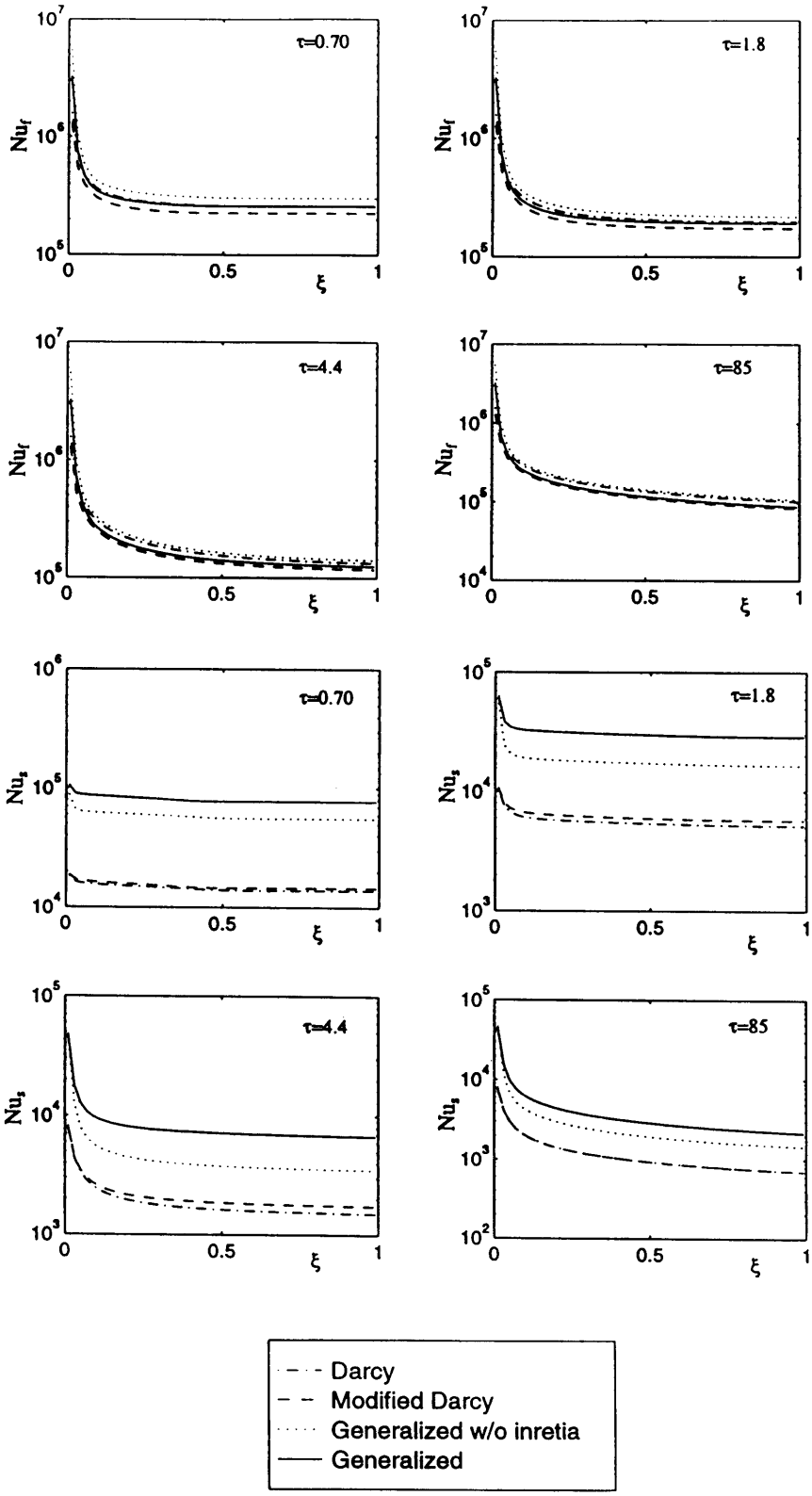

Fig. 5. Non-Darcian effects on the temporal fluid and solid phase Nusselt number for $\alpha_s/\alpha_f = 32$, $Da = 8.51 \times 10^{-8}$ and $Re_p = 40$.

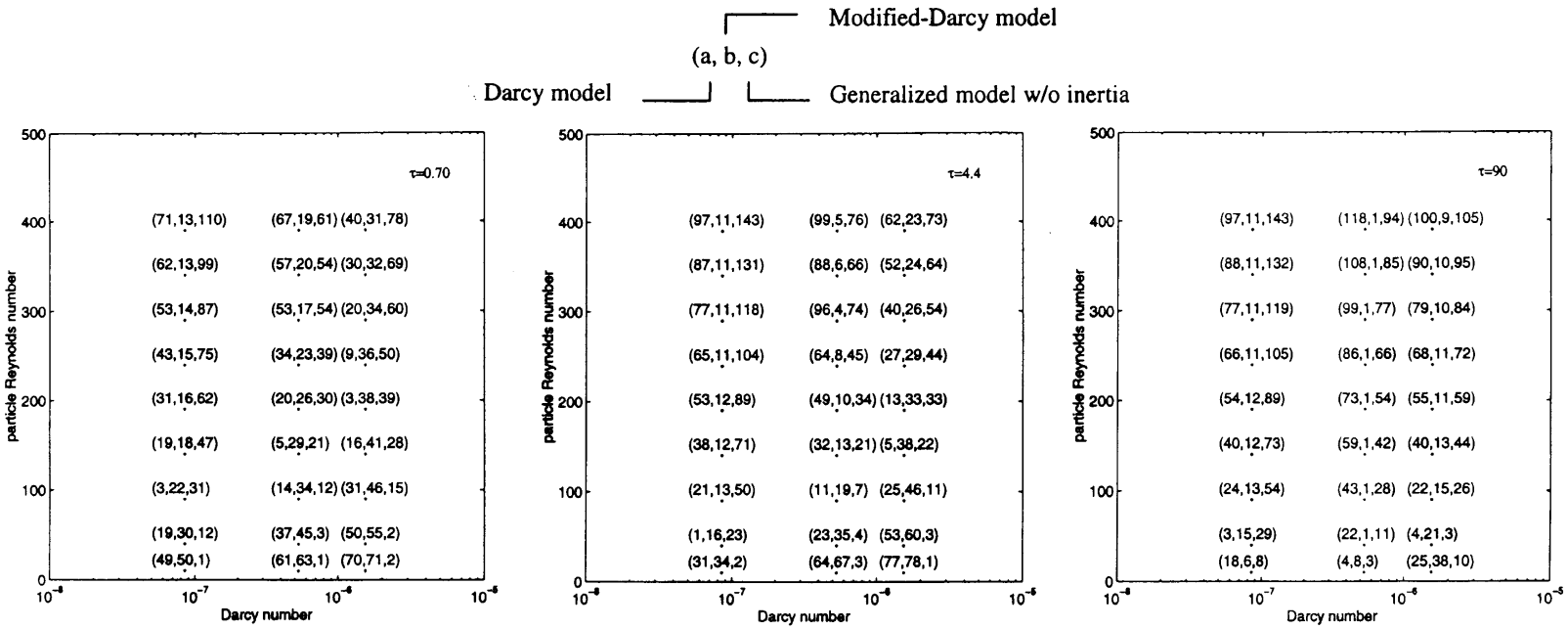

Fig. 6. The percentage error in the total Nusselt number neglecting the non-Darcian effects using $\alpha_s/\alpha_f = 32$.

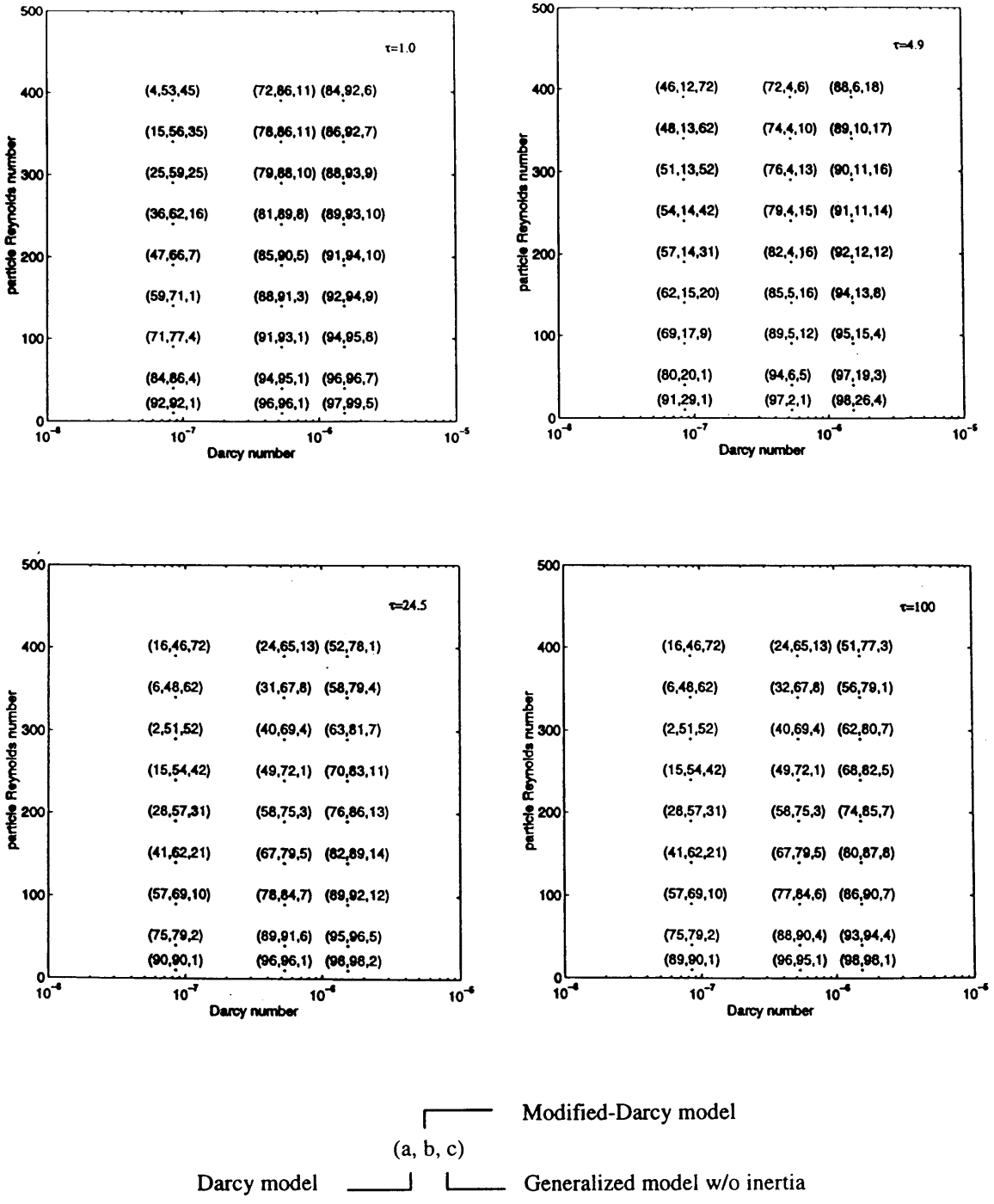

Fig. 7. The percentage error in the total Nusselt number neglecting the non-Darcian effects using $\alpha_s/\alpha_f = 2256$.

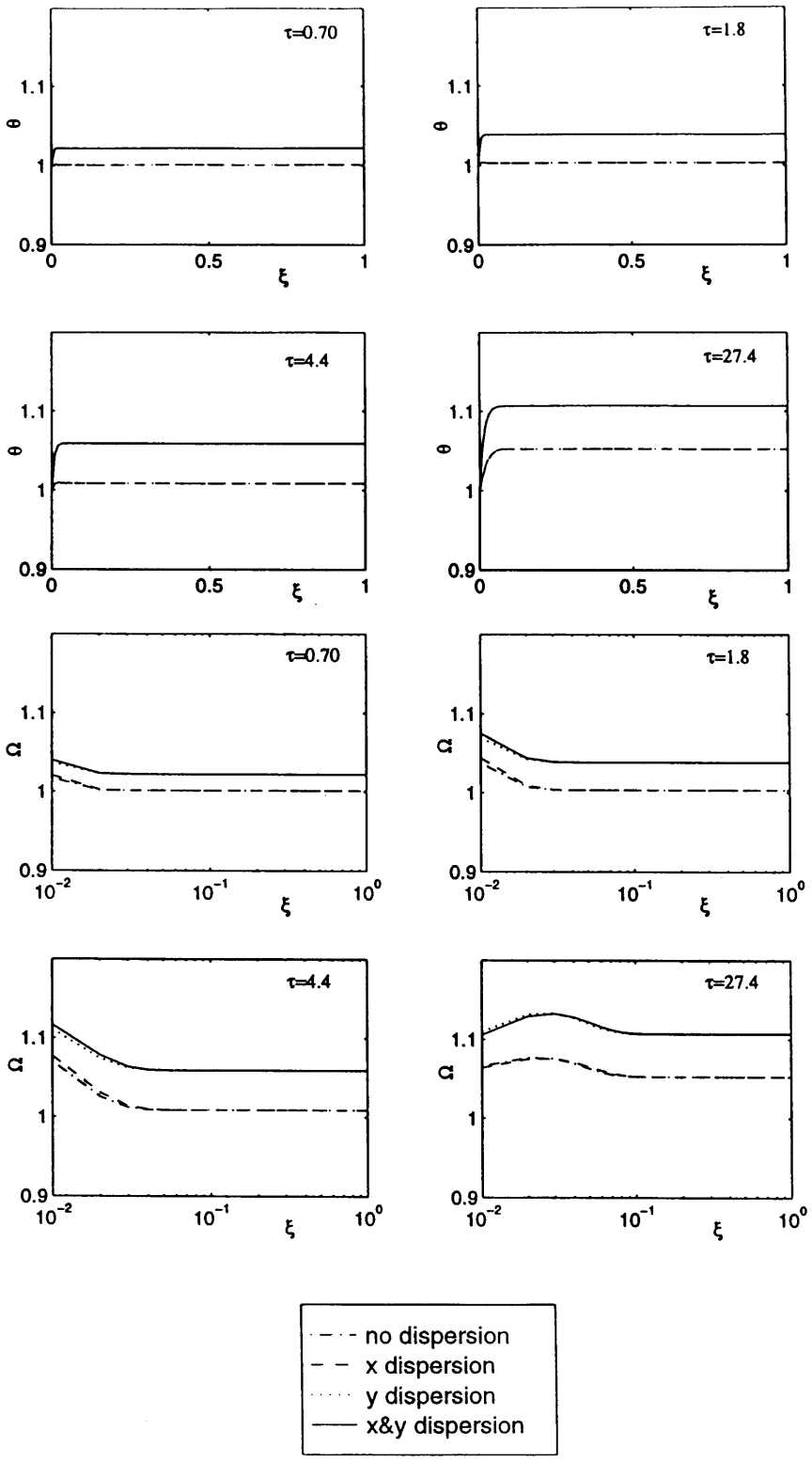

Fig. 8. Effect of thermal dispersion on the temporal fluid and solid phase temperature distribution for $\alpha_s/\alpha_f = 343$, $Da = 5.32 \times 10^{-7}$ and $Re_p = 190$.

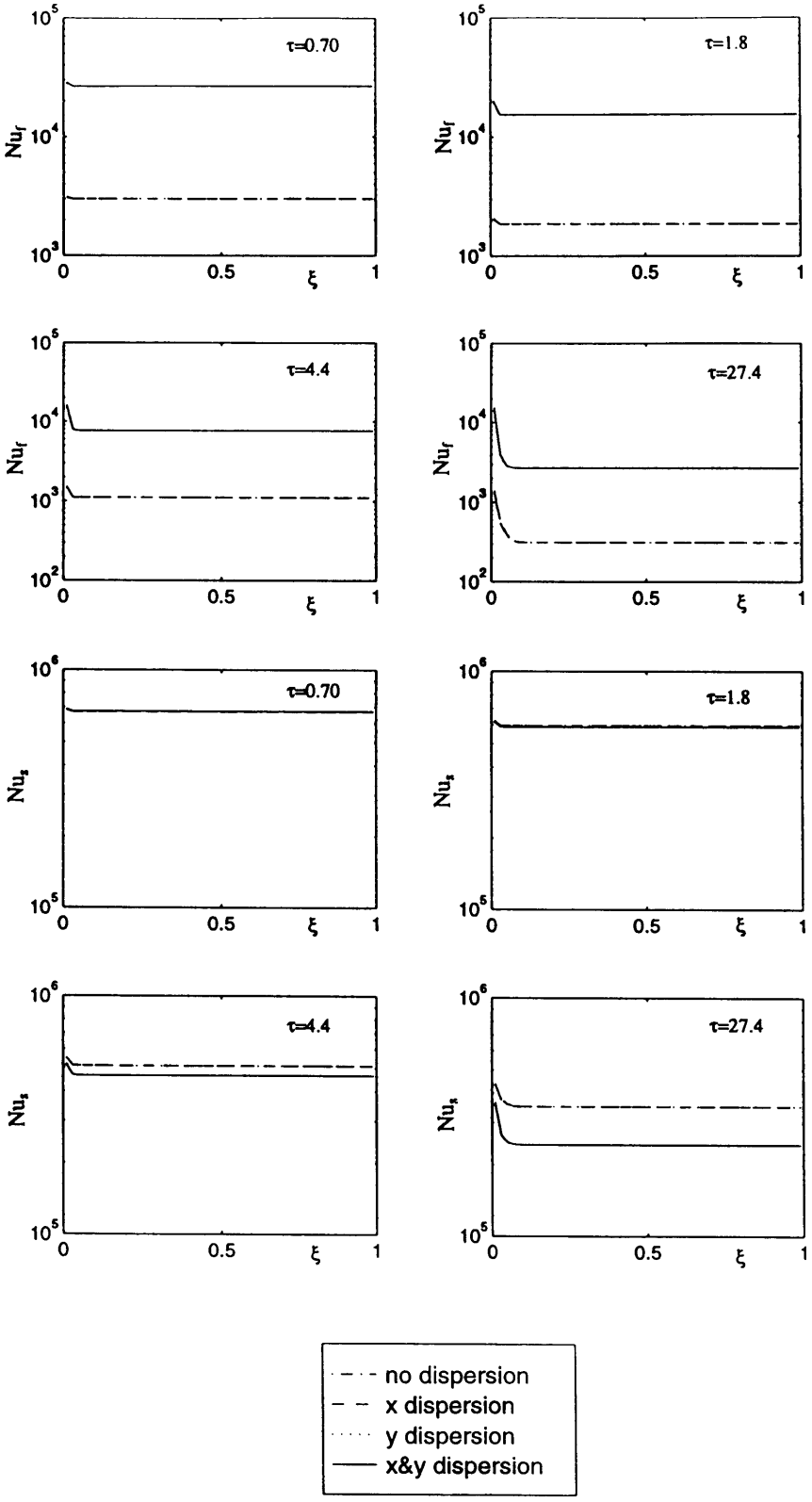

Fig. 9. Effect of thermal dispersion on the temporal fluid and solid phase Nusselt number for $\alpha_s/\alpha_f = 343$, $Da = 5.32 \times 10^{-7}$ and $Re_p = 190$.

moves toward the center of the bed where better mixing is achievable. The thermal dispersion effect on Nusselt number estimation is negligible for $\tau < 2.5$. This is attributed to the small magnitude of the velocity at the early stage and, consequently, the insignificance of the dispersion conductivity.

The results indicate that the longitudinal thermal dispersion has no significant contribution to the overall temporal thermal response of the packed bed especially at higher values of flow condition. It should be pointed out that the minute effect of the longitudinal thermal dispersion on Nusselt number predictions cannot be depicted in Fig. 9 since the Nusselt number results had to be plotted on a logarithmic scale due to the large variation in the magnitude between the different considered models.

An error map is presented to examine the significance of the longitudinal and the transverse thermal dispersion effects on a broad range of Da and Re_p. The generalized model that incorporates the thermal dispersion effects in both directions was taken as a reference. The comparisons were carried out with the simplified models that lack the dispersion effects in one or both coordinates. The percentage error was computed in a similar manner to that of the earlier error maps. These comparisons are illustrated in Fig. 10 for α_s/α_f equals to 343 for τ equals to 1.8, 4.4 and 27.4. The numbers between the parentheses represent the estimated error in dropping the dispersion effects from both coordinates, the axial coordinate and the vertical coordinate respectively at a given τ. As may be seen from the figure, the longitudinal dispersion is insignificant during the transient state for Re_p values between 10 and 400. This is attributed to the fact that the transverse thermal conductivity is the major source for the growth of the thermal boundary layer and also since the heat is transferred through the wall in a normal direction to the flow. It is doubtful that the longitudinal thermal dispersion will play a more significant role for α_s/α_f other than 343 under transient conditions. In addition, the results show that the magnitude of the estimated errors tend to increase at larger values of Re_p. Also, the magnitude of the errors were found to increase as time progressed. Furthermore, the errors increase to asymptotic values indicating that steady state conditions are approaching.

4.3. *Local thermal equilibrium assumption (LTE)*

The examination of the LTE condition was performed by computing the local temperature difference between the fluid and the solid at any given time. The maximum difference between the two phases was computed as follows:

$$\%\mathrm{LTE} = \frac{\max|T_{f(i,j)} - T_{s(i,j)}|}{(T_w - T_{in})} \times 100. \tag{20}$$

Numerical investigation of the temporal LTE condition was carried out for most of the materials considered in the analysis. The computational runs revealed that the LTE condition could be better monitored by the conductivity ratio k_s/k_f. Figure 11 displays the temporal LTE condition for the range of Da and Re_p considered in the analysis. The temperature discrepancy between the fluid and the solid phase was found to increase at early time since each phase responds differently due to the abrupt change in temperature condition at the entrance.

As time progresses, the temperature difference between the two phases reduced due to mixing, allowing for more effective exchange of energy between the two phases. The time corresponding to the maximum deviation from the LTE condition was found to be unique for each k_s/k_f. In addition, a larger discrepancy between the two phases was encountered at early times as the k_s/k_f ratio approach unity. However, this discrepancy quickly died down as time progressed making the temperature difference to be the smallest for the k_s/k_f ratio closest to unity. Although the LTE condition was found to improve with time, all the cases considered exhibited either poor or very poor LTE condition according to the qualitative rating reported in Amiri and Vafai [19].

Figure 12 demonstrates the temporal LTE condition for k_s/k_f equal to 12. As could be concluded from the figure, the LTE condition improves provided that ample time has elapsed. Moreover, the LTE condition appears to become more justifiable for small Da numbers. The results clearly show that the k_s/k_f ratio is a necessary condition for LTE assumption but not a sufficient one. The flow condition and the bed characteristics should be taken into consideration since they play an important role in making such an assumption acceptable or not.

4.4. *The transient two-dimensionality thermal behavior of a packed bed*

The validity of the one-dimensional approach for transient problems was also examined in this work. This was achieved by comparing the fluid phase centerline temperature against the local fluid temperature along the same vertical section. The inspection was carried out at the exit of the packed bed where the thermal boundary layer reaches its maximum and thus its utmost two-dimensional growth. Only the fluid phase results are shown here for brevity. The assessment of the two-dimensional strength was evaluated in two steps. First, a table was generated for the temperature percentage difference between the centerline fluid temperature at the exit and all the local fluid temperatures at the same section as follows:

$$\%\Delta T_f = \frac{|T_f(L,y) - T_f(L,H/2)|}{(T_w - T_{in})} \times 100. \tag{21}$$

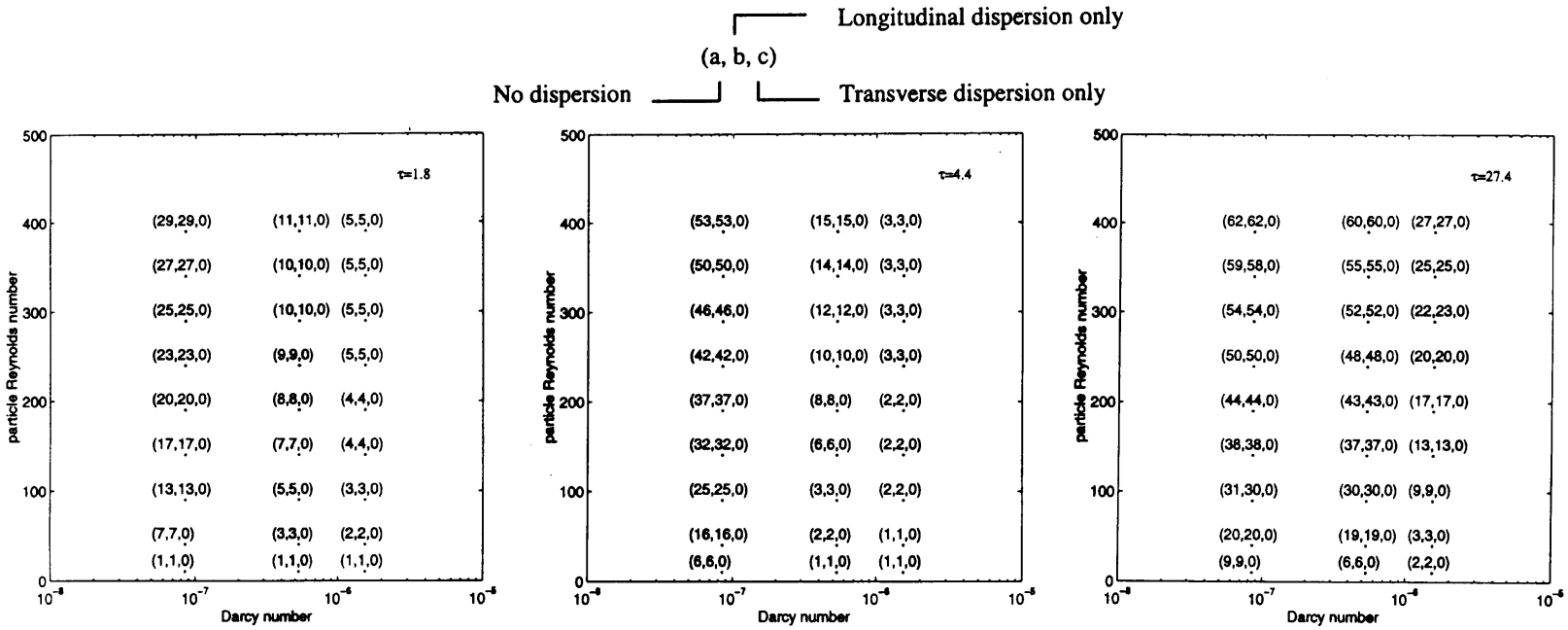

Fig. 10. The percentage error in the total Nusselt number for neglecting the thermal dispersion effects using $\alpha_s/\alpha_f = 343$.

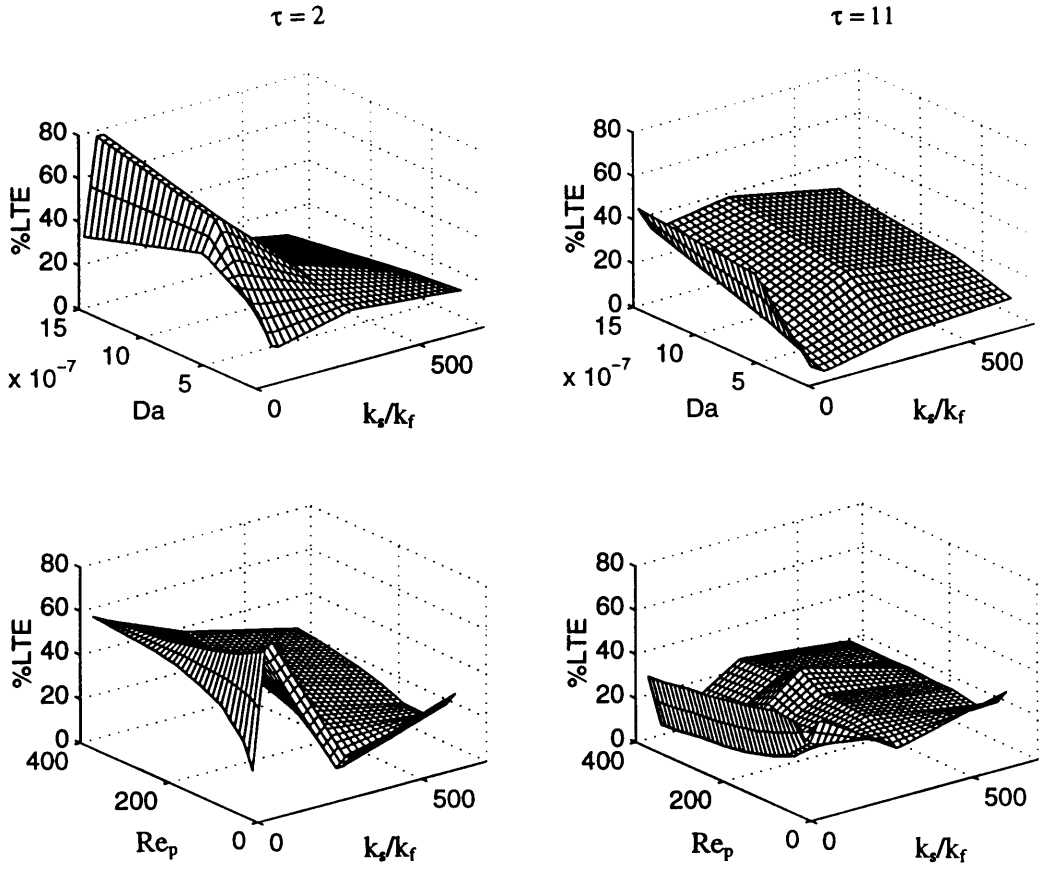

Fig. 11. The instantaneous LTE condition for τ equals 2 and 11.

Taking the centerline as the baseline and marching downward, the height where $\%\Delta T_f$ first exceeds 2.0 was measured. Second, the strength of the two-dimensional thermal behavior was computed from

$$\%2\mathrm{D} = \frac{y(\text{recorded location})}{H/2} \times 100. \tag{22}$$

Figures 13–15 display the strength of the two-dimensional thermal behavior under transient condition. The figures are presented for the cases of α_s/α_f equal to 2.1, 343 and 2256. Since mapping the entire range of Da and Re_p would require exhaustive numerical runs, some interpolation was found necessary to make up for the few locations where data were not available. The figures imply that the two-dimensionality effect increases with time indicating the continuous growth of the thermal boundary layer. In addition, this strength continues to increase but at a lower pace, which signals that steady state condition is reached. It is noted that the increase in Re_p for a fixed Da increases the two-dimensionality behavior. The same observation is extended to the increase in Da while Re_p remains constant. Moreover, the results do indicate that two-dimensional effects weaken as α_s/α_f approaches unity making α_s/α_f an appropriate tool, along with Da and Re_p, in examining the two-dimensional behavior of heat transfer in a packed bed.

5. Conclusions

The current investigation aims at studying the transient incompressible flows in a randomly packed bed of spheres. Along with the generalized momentum equation, a two-energy equation model is used to describe the thermal response of a packed bed. In addition, the temporal impact of the non-Darcian terms and the thermal dispersion effects on energy transport is explored over a broad range of pertinent non-dimensional parameters by means of error maps. A closer examination of the LTE condition revealed that the k_s/k_f ratio is a more appropriate tool in defining the range of validity for LTE condition. However, the k_s/k_f ratio is considered a necessary condition but not a sufficient one for LTE condition.

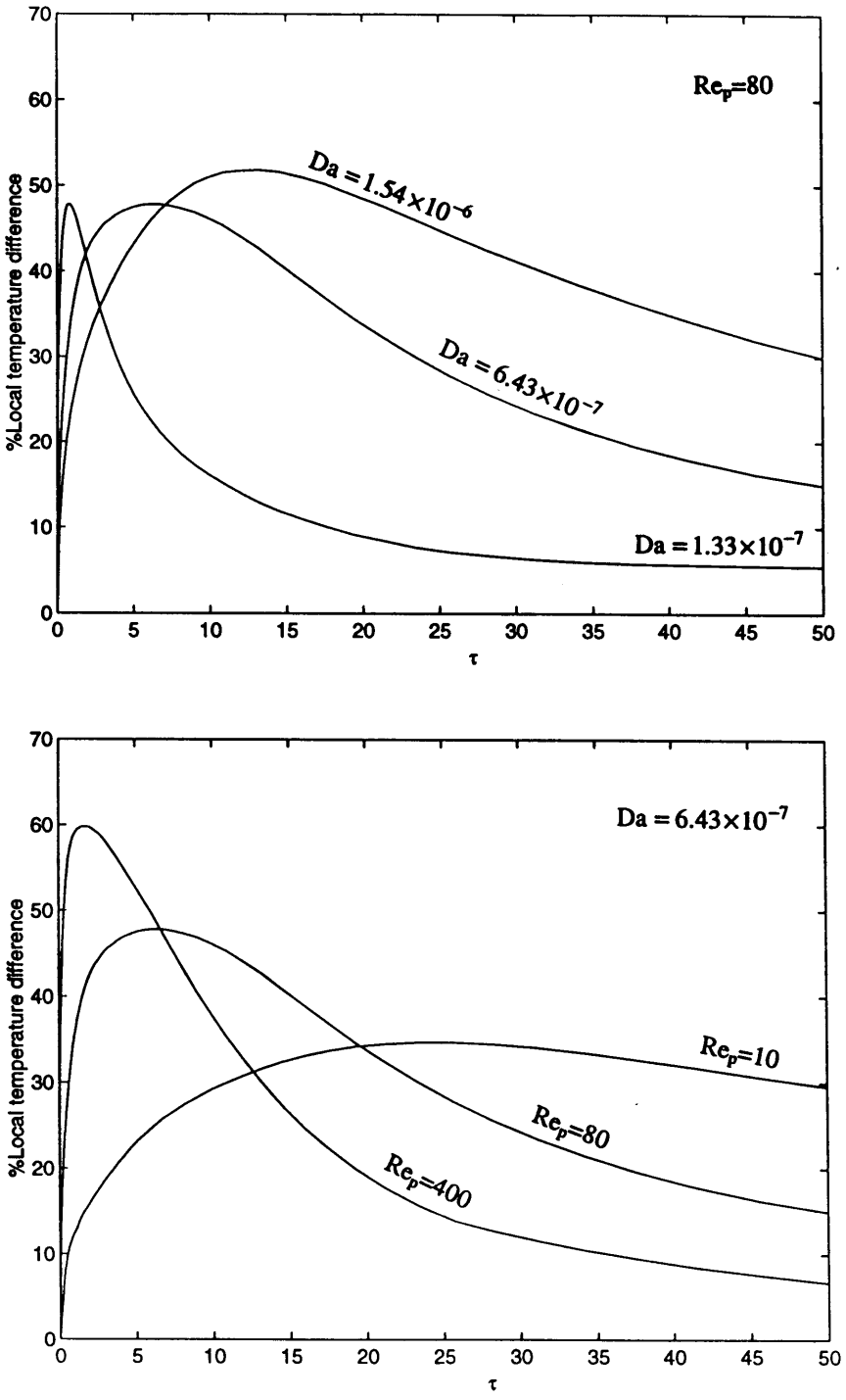

Fig. 12. The effects of Da and Re_p on the instantaneous LTE condition for $k_s/k_f = 12$.

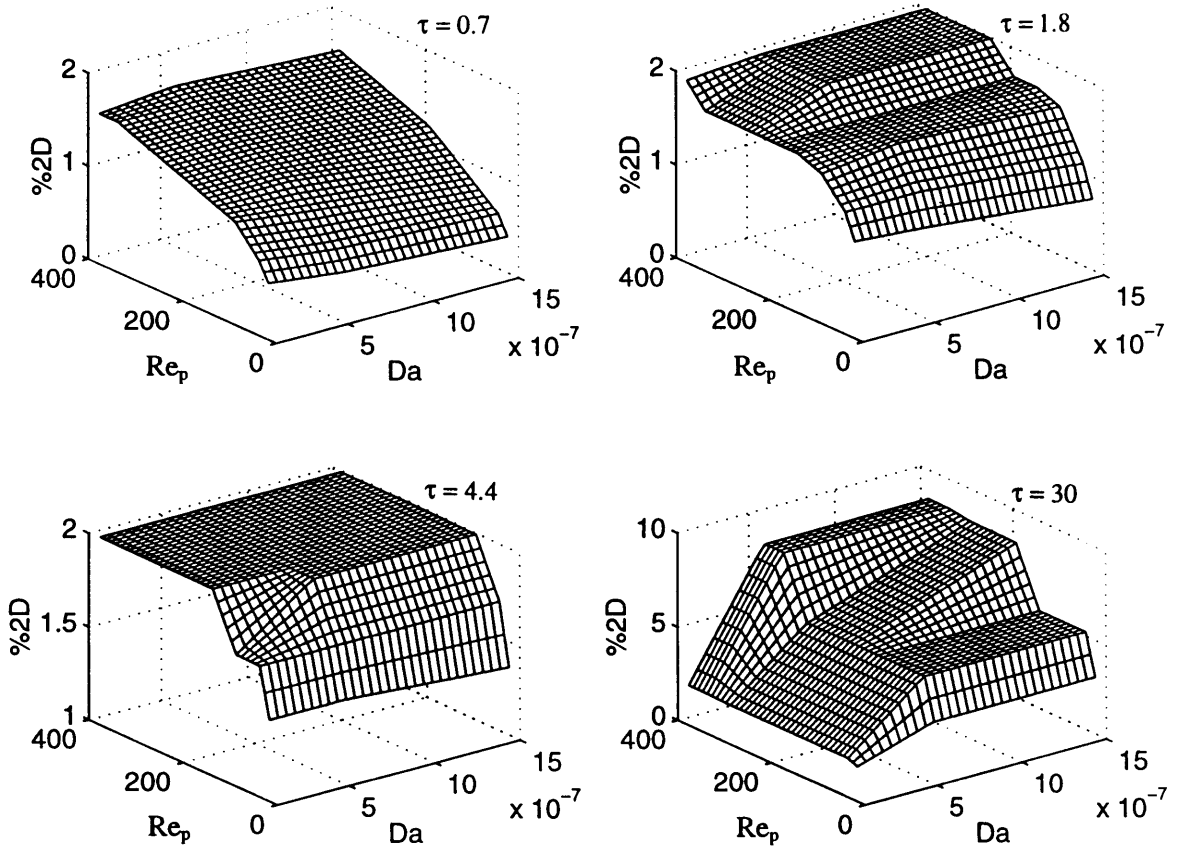

Fig. 13. The two-dimensionality strength for $\alpha_s/\alpha_f = 2.1$ at τ equals 0.7, 1.8, 4.4 and 30.

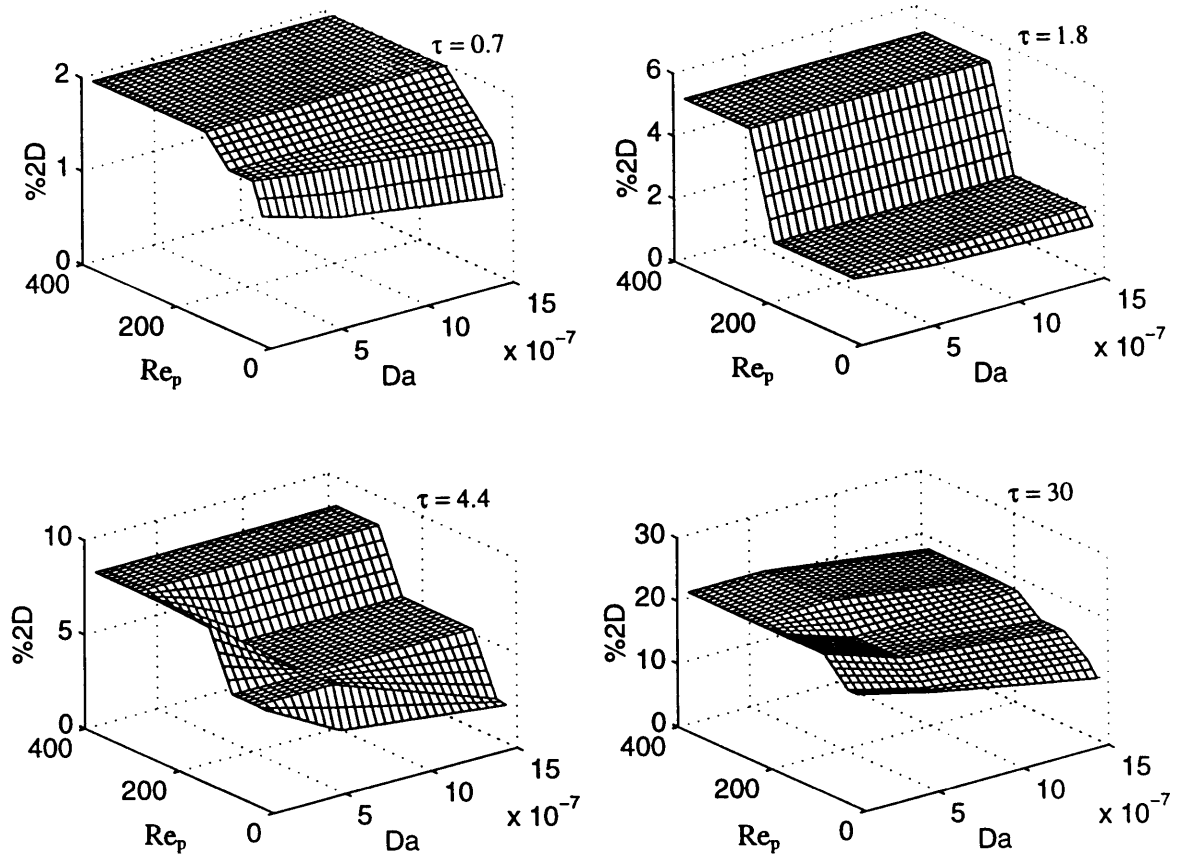

Fig. 14. The two-dimensionality strength for $\alpha_s/\alpha_f = 343$ at τ values of 0.7, 1.8, 4.4 and 30.

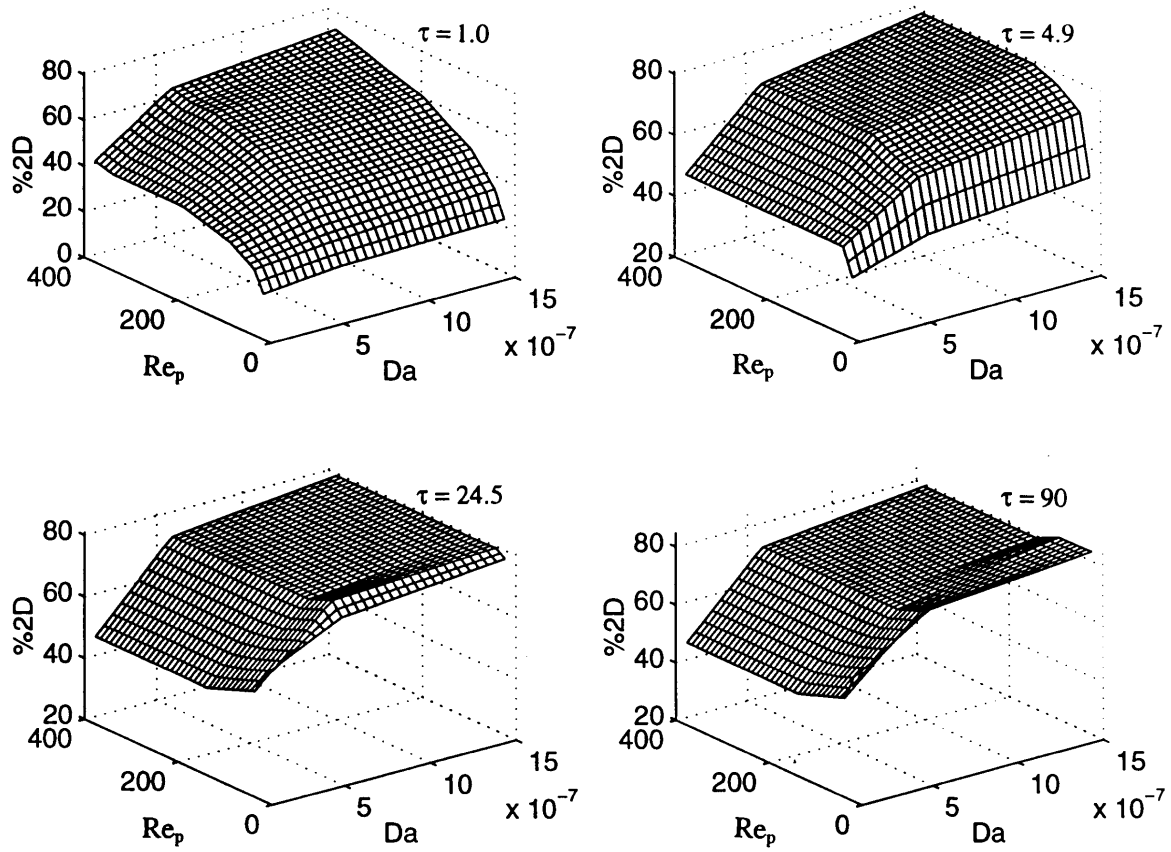

Fig. 15. The two-dimensionality strength for $\alpha_s/\alpha_f = 2256$ at τ values of 1.0, 4.9, 24.5 and 90.

Moreover, the temporal two-dimensional effects were studied and appeared to weaken for α_s/α_f closed to unity.

Acknowledgement

A grant from the Ohio Supercomputer center is acknowledged and appreciated.

References

[1] Tien CL, Vafai K. Convective and radiative heat transfer in porous media. Advances in Appl Mech 1989;27:225–81.
[2] Amiri A, Vafai K. Effects of boundary conditions on non-Darcian heat transfer through porous media and experimental comparisons. Num Heat Transfer 1995;27:651–64.
[3] Kuzay TM. Cryogenic cooling of X-ray crystals using a porous matrix. Rev Sci Instrum 1992;63(1):468–72.
[4] Vafai K, Tien CL. Boundary and inertia effects on flow and heat transfer in porous media. Int J Heat Mass Transfer 1981;108:195–203.
[5] Benanati RF, Brosilow CB. Void fraction distribution in beds of spheres. AIChE J 1962;4:450–64.
[6] Schwartz CE, Smith JM. Flow distribution in packed beds. Ind Engng Chem 1953;45:1209–18.
[7] Chadrasekhara BC, Vortmeyer D. Flow model for velocity distribution in fixed porous beds under isothermal conditions. Thermal Fluid Dynamics 1979;12:105–11.
[8] Vafai K. Analysis of the channeling effect in variable porosity media. J Energy Res Tech 1986;108:131–9.
[9] Vafai K, Alkire RL, Tien CL. An experimental investigation of heat transfer in variable porosity media. J Heat Transfer 1985;107:642–7.
[10] Kaviany M. Laminar flow through a porous channel bounded by isothermal plates. Int J Heat Mass Transfer 1985;28:851–8.
[11] Renken KJ, Poulikakos D. Experiment and analysis of forced convection heat transport in a packed bed of spheres. Int J Heat Mass Transfer 1988;31:1399–1408.
[12] Hunt ML, Tien CL. Non-Darcian convection in cylindrical packed beds. J Heat Transfer 1988;110:378–84.

[13] Yagi S, Kunii D. Studies on effective thermal conductivities in packed beds. AIChE J 1957;3(3):373–81.
[14] Wakao N, Kaguei S. Heat and mass transfer in packed beds. New York : Gordon and Breach Science Publishers Inc., 1982.
[15] Levec J, Carbonell RG. Longitudinal and lateral thermal dispersion in packed beds. AIChE J 1985;31(4):591–602.
[16] Gunn J, Desouza JFC. Heat Transfer and axial dispersion in packed beds. Chem Eng Sci 1974;29:1363–71.
[17] Vortmeyer D. Axial heat dispersion in packed beds. Chem Eng Sci 1975;30:999–1001.
[18] Sözen M, Vafai K. Longitudinal heat dispersion in porous beds with real gas flow. J Thermophysics Heat Transfer 1993;7(1):153–7.
[19] Amiri A, Vafai K. Analysis of dispersion effects and non-thermal equilibrium, non-Darcian, variable porosity incompressible flow through porous media. Int J Heat Mass Transfer 1994;11(6):939–54.
[20] Wakao N, Kaguei S, Funazkri T. Effect of fluid dispersion coefficients on particle-to-fluid heat transfer coefficients in packed beds. Chem Eng Sci 1979;34:325–36.
[21] Koch DL, Brady FJ. Dispersion in fixed beds.J Fluid Mech 1985;154:399–427.
[22] Schumann TEW. Heat transfer : a liquid flowing through a porous prism. J Franklin Inst 1929;208:405–16.
[23] Beasley DE, Clark JA. Transient response of a packed bed for thermal energy storage. Int J Heat Mass Transfer 1984;27(9):1659–69.
[24] Vafai K, Amiri A. Non-Darcian effects in confined forced convective flows. To appear in Transport phenomena in porous media. England : Elsevier Science.
[25] Whitaker S. Simultaneous heat, mass and momentum transfer in porous media : a theory of drying. Advances in Heat Transfer 1977;13:119–203.
[26] Ergun S. Fluid flow through packed columns. Chem Engng Progress 1952;48:89–94.
[27] Vafai K. Convective flow and heat transfer in variable porosity media. J Fluid Mech 1984;147:233–59.
[28] Dullien FAL. Porous media fluid transport and pore structure. New York : Academic Press, 1979.
[29] Riaz M. Analytical solution for single- and two-phase models of packed-bed thermal storage systems. J Heat Transfer 1977;99:489–92.